First-principles modeling of superlattice intrinsic stacking fault energies in Ni3Al based alloys

Breidi, Abed Al Hasan; Allen, Joshua; Mottura, Alessandro

First-principles modeling of superlattice intrinsic stacking fault energies in Ni_3Al based alloys

A. Breidi,* J. Allen, and A. Mottura
School of Metallurgy and Materials, University of Birmingham, Edgbaston B15 2TT, United Kingdom
(Dated: November 17, 2017)

High-throughput quantum mechanics based simulations have been carried out to establish the change in lattice parameter and superlattice intrinsic stacking fault (SISF) formation energies in Ni_3Al-based alloys using the axial Ising model. We had direct access to the variation in SISF energies due to finite compositional change of the added ternary transition metal (TM) element through constructing large supercells, which was equally necessary to account for chemical disorder. We find that most added TM ternaries induce an important quasi-linear increase in the SISF energy as a function of alloying composition x. The most pronounced increase corresponds to Fe addition, while Co addition decreases the SISF energy monotonically. Our results shed light on the role played by TM elements on strengthening $L1_2$ Ni_3Al precipitates against stacking fault shear. The data are of high importance for designing new Ni-based superalloys based on computational approaches.

Keywords: First-principles; Ni superalloys; Alloys; Stacking faults; Dislocations

I. INTRODUCTION

Nowadays high-performance aero-engines owe their exceptional high-temperature mechanical properties to Ni-based superalloys consisting of a large volume fraction of ordered γ' ($L1_2$) Ni_3Al precipitates coherently embedded in a matrix of γ-Ni (fcc Ni) phase[1]. The shear strength of these precipitates resulting from order strengthening and the anomalous temperature dependence of the yield stress (*critical resolved shear stress* CRSS) give rise to Ni-based superalloys extraordinary strength and deformation resistance at high-temperatures[2].

In contrary to the situation at high temperatures ($\geqslant$ 950 °C[3]) and low stresses where the micromechanism of creep is characterized by dislocations activity of type $a/2\langle 1\bar{1}0\rangle\{111\}$ restricted to the γ channels, experiments[3–5] have shown that at intermediate-temperatures (750 − 850 °C) and high stresses ($\geqslant$ 500 MPa) the micromechanism of creep is quite different. Reports in the literature[3–5] established that during the primary creep process the deformation occurs by shearing the γ' precipitates – so called *stacking fault shear* – by dislocation ribbons of overall Burgers vector $a\langle 11\bar{2}\rangle$ [3–5].

It was Leverant and Kear[6] who made the first observation that primary creep deformation occurs by the movement of dislocation ribbons of net Burgers vector $a\langle 11\bar{2}\rangle$, which was later supported by transmission electron microscopy (TEM) studies. Now it is known that the mechanism of formation of the $a\langle 11\bar{2}\rangle$ dislocation ribbons involves the reaction of $a/2\langle 1\bar{1}0\rangle\{111\}$ dislocations in γ, which are dissociated into their Shockley partials. A typical reaction might then be given by[5]

$$a/2[011] + a/2[\bar{1}01] \rightarrow a/3[\bar{1}12] + a/6[\bar{1}12] \tag{1}$$

If the applied stress is sufficient, the $a/3[\bar{1}12]$ dislocation is able to enter the γ', leaving a superlattice intrinsic stacking fault (SISF) behind it and the remaining $a/6[\bar{1}12]$ at the γ/γ' interface.

The SISF energy is known to play an important role in the structure and energetics of dislocations formed by slip processes. There is strong evidence that SISFs and SESFs, characterized by low fault-energies relative to other stacking fault configurations, are the main planar fault energies through which shearing of the γ' phase happens under high-applied-stress and low-intermediate-temperatures creep conditions[5, 7–9] (Primary creep). The knowledge of the variation of these fault energies upon alloying is extremely important to have a better understanding of the shearing of the strengthening γ' phase in nickel-base superalloys which is crucial for developing physics-based deformation models of the aerospace and power generation systems.

The transmission electron microscopy technique used to determine the planar fault energies is known to involve assumptions, and consequently produces sometimes inaccurate values, particularly for the SISF energies – see Ref. 10 and references therein. The experimental technique relies on measuring the width of the stacking fault ribbon which is inversely proportional to the fault energy[11–13]. Accordingly, it is accompanied by difficulties related to thin film effects, short length ribbons (comparable to errors) and uncertainty in applying corrections. Moreover, the experimental determination of fault energies depends heavily on the type of elasticity theory applied.

On the other hand, *ab initio* quantum mechanics based methods are powerful tools that can be harnessed to enhance the mechanical properties of complex multicomponent Ni-base superalloys *via* probing the variation of

*corresponding author; a.breidi@hotmail.com; Moved to: Theory and modelling department - Culham Centre for Fusion Energy.

the stacking fault energies upon adding a specific ternary element with composition x to the Ni_3Al based-systems. There are several factors giving rise to the complexity of Ni-base superalloys: the wide variety of alloying elements (as many as 10-15), the intricacy of the microstructure (two-phase mixture), and most importantly for this study is the chemical disorder. Investigating stacking fault energies while representing properly the chemical randomness is a big challenge due to the difficulty in modeling solid solutions and the high computational cost to perform the calculation. In the literature, there are few attempts to approach this issue but they are done on model systems and not in a systematic way.

The aim of this study is to address how the chemical disorder influences SISF energies in Ni_3Al-based alloys through employing a wide variety of transition metal (TM) elements. We try to establish the evolution in SISF energy as a function of alloying composition x. The main issues we tackle: Is the nature of the variation of SISF energy in Ni_3Al-based pseudo-binary alloys similar to that in Ni-based binary alloys? Are the magnitudes of the SISF energies smaller or greater than those of anti-phase boundary (APB) at similar compositions? Do different alloying elements display important different effects on the SISF energy? Does the change in SISF energies in the studied pseudo-binary systems offer the possibility to fine-tune the SISF energies of a multicomponent alloy and thereby optimizing creep resistance?

In fact, the SISF energies calculation and their accuracy depend heavily on the lattice parameters of the pertinent alloys. Hence, we carefully model the variation of the lattice parameter in Ni_3Al based alloys.

II. SISF ENERGY INVESTIGATION METHODOLOGY

The SISF energy is the energy cost needed to shear two adjacent atomic planes in a crystal lattice relative to each other. There are two methodological approaches to explore the alloying effect on the SISF energies of Ni_3Al. The most complex one is where one shears two parts of a pristine supercell with respect to one another along a specific plane with a relative displacement x. This gives rise to the concept of conventional generalized stacking fault energy (GSF)[14], known as γ_{GS} or γ-surface. The superlattice intrinsic stacking fault energy corresponds to a particular point on the γ-surface, the minima in the strain-energy versus relative-displacement x curve with x assuming a specific partial Burgers vector, thereby called stable stacking fault. The unstable stacking fault energy, a crucial parameter in determining the ductility of the material[15], corresponding to the first maximum in the strain-energy versus relative-displacement x curve, is reached before the SISF.

The second approach is the axial Ising model[16] (AIM) where the SISF energy is determined directly from a series expansion of different infinitely repeated defect-free stacking sequences. In the first order only $L1_2$ and $D0_{19}$ stacking sequences are considered, while higher-order expansions involve more complex phases. The major advantage of using this approach is its reasonable computational cost in comparison with the highly time demanding supercell approach where the the stacking fault is explicitly considered. Hence, the AIM model provides a robust tool to qualitatively estimate the variation in SISF energies upon alloying and variation due to magnetic fluctuation[17–24]. A further advantage of the AIM model is the feasibility and straightforwardness of considering the temperature effects, due to applicability of including bulk lattice, magnetic and electronic excitations[23–25].

However, there exist some disadvantages from using this model. One cannot account for certain effects induced by the stacking fault formation such as: changes in the local magnetic order, spatial atomic arrangement, segregation of impurities phenomena known as Suzuki and anti-Suzuki effects[26–28]. Moreover, one cannot probe with this model the changes in chemical order occurring near the fault and the energetic barriers related to the formation of SISF. The supercell approach treats explicitly the energetic barriers needed to be overcome in order to realize the SISF, thus averting the abovementioned disadvantages presented by the AIM model. However, the use of the supercell approach comes with a high price; it demands large computing time due to the large supercell designed to describe the fault. As far as Ni-based materials are concerned, this method has been applied to calculate planar fault energies in pure $L1_2$ compound Ni_3Al[29], fcc Ni[30], Ni_3Al dilute alloys[29, 31], and few Ni_3Al-based alloys[32].

In fact a proper representation of the chemical disorder in Ni_3Al real alloys demands large configurational space on its own - a simple atomistic description of random alloys based on a statistical distribution of atoms represents a serious challenge. Considering the fact that we are interested only in estimating the magnitude of the SISF energies in Ni_3Al based random solid solutions and not the complete information of the γ-surface, we have decided to employ the AIM model, thereby avoiding an additional increase in the size of the supercell as imposed by the supercell approach. It should be mentioned within this context that Yu and Wang[29] have earlier applied the supercell approach to study few Ni_3Al dilute alloys with five ternary elements; however they have introduced the ternary element as a single impurity, substituting an Al atom in the slip plane, which does not account for the random distribution of atoms on the Al sublattice. Therefore their studied systems lack the realistic representation of chemical disorder and subsequently cannot be regarded as random solid solutions.

The detailed methodology of the AIM is explained elsewhere[13, 16, 33]. There are two implementations of the AIM: the axial nearest-neighbor Ising model (ANNI) and the axial next-nearest-neighbor Ising model (ANNNI). The ANNNI model, involving three struc-

tures $L1_2$, $D0_{19}$ and $D0_{24}$, is sufficient as interactions are generally very short in range in metals[34]. The ANNI model, involving only $L1_2$ and $D0_{19}$ structures, has proven to produce similar values to the ANNNI model. The (111) SISF formation energy of $L1_2$ alloys using the axial nearest-neighbor Ising model (ANNI) is given by

$$\gamma_{\mathrm{ANNI}}^{L1_2} = \frac{8(E_{D0_{19}} - E_{L1_2})}{V_{L1_2}^{2/3} \cdot \sqrt{3}} \quad . \tag{2}$$

where V_{L1_2} is the volume of 4-atoms $L1_2$ unit cell and $V_{L1_2}^{2/3} \cdot \sqrt{3}$ is the area of 4-atoms in the $L1_2$ (111) plane over which the stacking fault extends. E_{L1_2} and $E_{D0_{19}}$ are the energies per atom of the $L1_2$ and $D0_{19}$ structures.

III. COMPUTATIONAL METHOD

A. Modeling pseudobinary alloys

We describe γ' Ni_3Al-based alloys as pseudobinary systems where Ni and Al atoms occupy exclusively their *own* sublattices and the added TM ternary element X occupies either Ni or Al or both sublattices simultaneously, specifically: (a) $Ni_{0.75-x}X_xAl_{0.25}$ or (b) $Ni_{0.75}Al_{0.25-x}X_x$ or (c) $Ni_{0.75-x}Al_{0.25-x}X_{2x}$; X belongs to $3d$, $4d$ and $5d$, while x is the alloying composition. The studied range of values of x is limited to the experimental solubility of X in Ni_3Al alloys[35].
The pseudobinary systems $Ni_{0.75}Al_{0.25-x}X_x$ and $Ni_{0.75-x}Al_{0.25-x}X_{2x}$ are both modeled using 256-atom $L1_2$-based 4×4×4(×4-atoms) and $D0_{19}$-based 4×4×2(×8-atoms) supercells, whereas $Ni_{0.75-x}X_xAl_{0.25}$ system is modeled using 128-atom $L1_2$-based 4×4×2(×4-atoms) and $D0_{19}$-based 4×2×2(×8-atoms) supercells.[36] The supercells were generated to reproduce chemical disorder in alloys neglecting the contribution from possible short-range order effects. We have minimized the Warren-Cowley short-range order (SRO) parameters[37, 38] at several nearest neighbor coordination shells to guarantee random distribution of atoms. We provide the supercells as supplementary materials.
As implied in their chemical formulas, our alloys are stoichiometric, nonstoichiometric alloying occurs on either one or at both sublattices separately. Ni-antisites and vacancies are not accounted for in this study. The added ternary elements have experimentally[35, 39, 40] and theoretically[41–43] proven to show strong site preference to either one of the sublattices or equally to both. Additionally, this preference for some elements, namely, Mn, Fe, Co, Cu, Ag and Au, changes depending on the Ni_3Al phase composition[42]. Accordingly, the TM element X has been assigned to Ni or Al or both sublattices in accordance with experiment[35] and theory[41–43].

B. First-principles techniques

Density–functional theory[44, 45] DFT was employed to perform the first-principles calculations. The total energies and forces were calculated using the Projector Augmented Wave method, implemented in the Vienna Ab initio Simulation Package (VASP)[46–48]. The exchange–correlation (XC) energy of electrons is described in the generalized gradient approximation (GGA) using the functional parameterization of Perdew–Burke–Ernzerhof[49]. Necessary convergence tests were made to control the stability of energy differences between $L1_2$ and $D0_{19}$ phases, where the energy cut–off, a crucial parameter of calculation for the PAWs, was set to 350 meV. This was enough to guarantee the uncertainty in SISF energy to be less than 2 mJ/m^2. A mesh of a 36, 32, 68, and a 74 special **k**-points for 256-Atom $L1_2$, 256-Atom $D0_{19}$, 128-Atom $L1_2$, and 128-Atom $D0_{19}$, respectively, were taken in the irreducible wedge of the Brillouin zone for the total energy calculations. The convergence tests for the plane–wave cutoff and the number of the **k**-points were essential to assure reliable total energy differences. Whilst relaxing the $L1_2$ phase we have intentionally kept its spacegroup fixed. That was feasible by keeping the supercell shape fixed (no cell shape relaxation was allowed) while minimizing $L1_2$ total energy. In this way, a spontaneous lowering of the symmetry from a high symmetric phase was not possible. The $L1_2$ volume was equilibrated, assuming a zero–pressure environment, through successively carrying out a set of volume optimization and local atomic relaxations, until no further change in total energy was observed. Regarding the $D0_{19}$ phase, we emphasize that the total energy was minimized, through performing only local atomic relaxations at the corresponding $L1_2$ equilibrium volume-per-atom and at fixed $D0_{19}$ ideal c/a ratio, in this way we guaranteed that $a_{D0_{19}}$ and $c_{D0_{19}}$ correspond to the underlying $L1_2$ lattice, *i.e.*, $a_{D0_{19}}/a_{L1_2} = \sqrt{2}$ and $c_{D0_{19}}/a_{L1_2} = \sqrt{4/3}$. The atomic positions for both phases were relaxed using the conjugate gradient algorithm[50], a highly recommended scheme to relax the atoms into their instantaneous ground state, especially in case atomic relaxation is problematic.

C. Magnetism

It is known that Ni_3Al is a weak itinerant ferromagnet with very low Curie temperature T_c=41.5 K[51] (ferromagnetic to paramagnetic transition). Adding a transition metal element to Ni_3Al may render it paramagnetic at already 0 K or enhance and extend its ferromagnetic state up to higher temperatures, such as in $Ni_{0.75-x}Al_{0.25-x}Fe_{2x}$[52] where T_c increases from 41.5 K for the Fe-free to 410 K for the limiting concentration of 12 at. % Fe in the $L1_2$ structure. At intermediate temperature ranges (800-1100 K), most likely all Ni_3Al based alloys will be in the paramagnetic state. Let us note here

that at the abovementioned temperatures the local magnetic moment on Ni can survive due to longitudinal spin fluctuations LSF[53].
Considering the difficulties associated with determining the SISF energies of alloys in their paramagnetic state, we have decided to do spin-polarized (SP) calculations. We believe that a PAW spin-polarized scheme, allowing relaxation of local magnetic moments on the different atoms of an alloy, while not imposing a zero total-magnetization, can yield a close picture, of the change in SISF energies, to what one can get with an exact treatment of the high temperature paramagnetic phase.

IV. RESULTS

A. Lattice parameters

The dispersion strengthening and the morphology of γ' precipitates are mainly controlled by the lattice misfit between γ and γ' phases in Ni-base superalloys. The effect of composition on lattice parameter is indispensable to determine the misfit between γ and γ'. The sign and magnitude of the misfit between both phases are known to control microstructural evolution during creep and thus creep behavior[54, 55]. Consequently the knowledge of the lattice parameter upon introducing a transition metal solute X into either Ni or Al-sublattice, with finer compositional changes x close to the stoichiometric Ni_3Al γ' phase is indispensable to establish trends facilitating the design and characterization of new commercial superalloys. The induced-change in the lattice parameter of Ni_3Al has been investigated experimentally and theoretically in a number of papers, whereby the experimental studies[35, 56, 57] include specific solutes only, and the theoretical calculations are rare and concern particular model alloys.
Making use of *ab initio* quantum mechanics based methods, which have proved to be quite reliable in predicting structural and thermodynamic properties of alloys[58], we try to establish and understand the dependence of the lattice parameter, in Ni_3Al based alloys, on the alloy composition, using an exhaustive number of the transition metals TM atoms as alloying ternary elements.

1. *Experimental situation*

The available experimental data[35, 56, 57] are, unfortunately, scarce and concern only several investigated compositions of quite few alloys. Mishima *et al.*[35] prepared Ni_3Al alloys with ternary transition elements by arc-melting and homogenized the samples at 1273 K and 1423 K (for Ta and Nb) and then furnace cooled to ambient temperature. Additionally, they made use of rare number of data available – see Ref.35 and references therein. They argue that the alloy additions were chosen

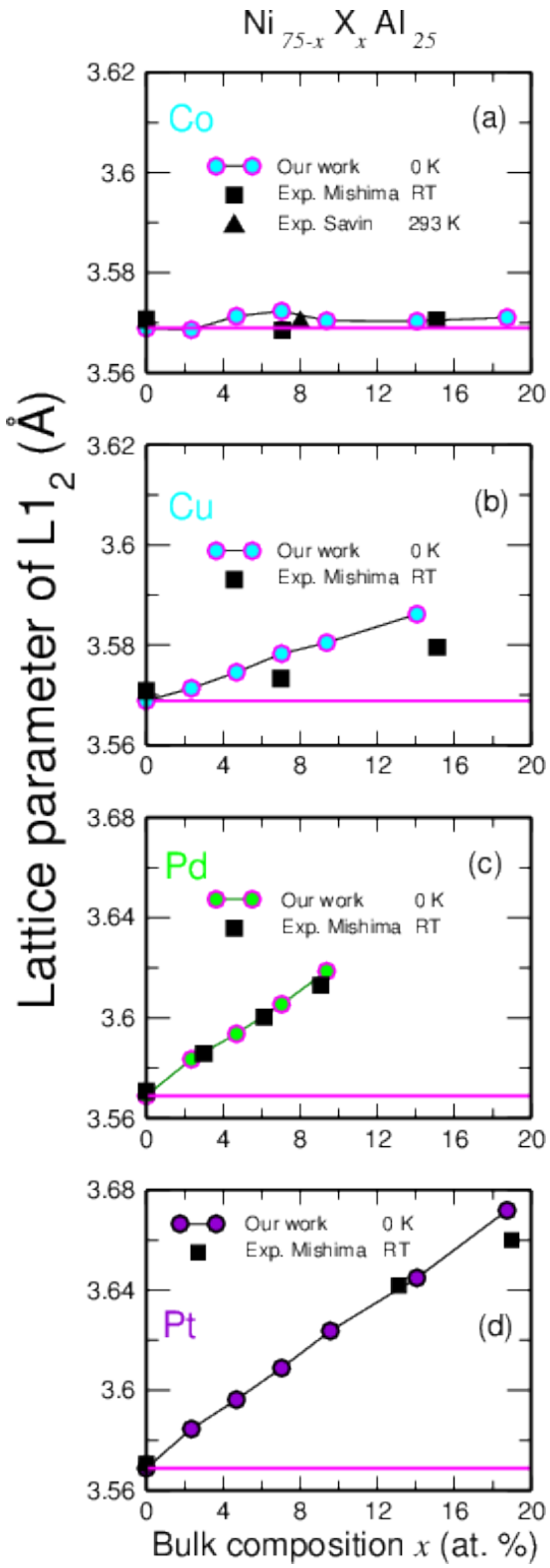

FIG. 1. Change in the equilibrium lattice parameter of the alloy $Ni_{75-x}X_xAl_{25}$ as a function of the ternary element composition x (at. %). The available experimental (RT[35] and 293 K[57]) data are also shown. The lines connecting the points are only to help guiding the eyes through the data.

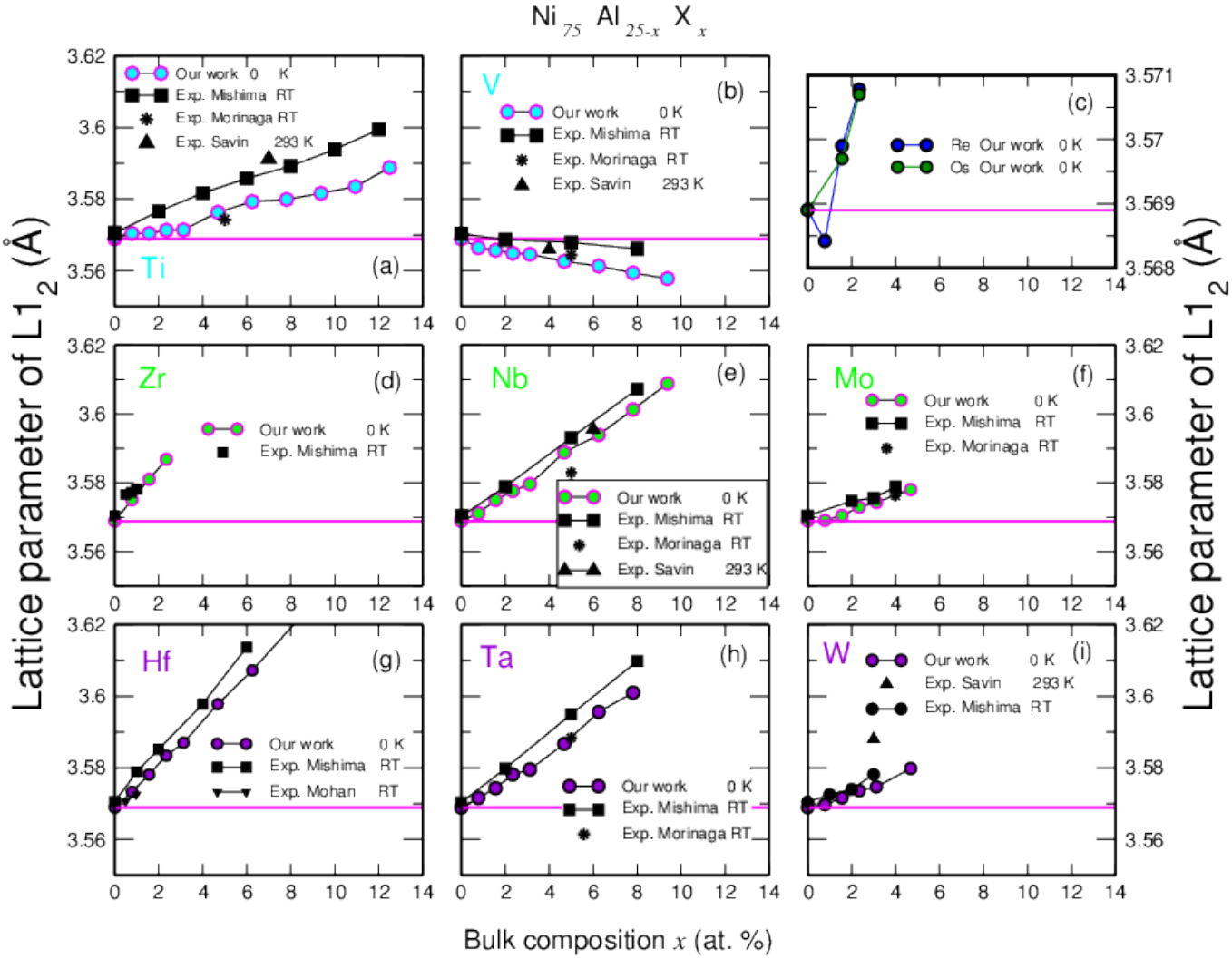

FIG. 2. Variation in the equilibrium lattice parameter of the alloy $Ni_{75}Al_{25-x}X_x$ as a function of the ternary element composition x (at. %). Within each panel, we present the available experimental data (RT[35, 56, 59] and 293 K[57]). The lines connecting the points are only to help guiding the eyes through the data.

so that the increase in alloying element is along the direction that gives the maximum solubility of γ' in each ternary phase diagram, subsequently the authors present that Co, Pd, Pt and Cu substitute for Ni-sites, while Ti, Zr, Hf, V, Nb, Ta, Mo and W substitute for Al-sites.

In contrast to Ref. 35, Morinaga *et al.*[56] grew $L1_2$ single crystals containing Ti, V, Cr, Mn, Fe, Nb, Ta and Mo using the Bridgman method. These crystals were heat treated at 1273 K and rapidly quenched in water. The composition of each alloying element X was then determined to be *about* 5 at. % for all crystals except that for Ni_3(Al,Mo) it was *about* 4 at. %. The authors[56] clearly state that the refinements with respect to the occupation number were tried without success, therefore the following model has been adopted: (1) When the Ni concentration exceeds 75 at. %, the Ni sublattice is completely filled, and the rest of Ni along with Al and alloying element X occupy the Al sublattice. (2) When the Ni concentration is smaller than 75 at. %, the excess sites in the Ni sublattice are filled with compositionally averaged Al and X atoms. The Al sublattice is occupied by the rest of the Al and X atoms. According to this assumption, all the considered alloying elements partition mostly to the Al-sublattice as Ni composition is close to 75 at. %.

On the other hand, Savin *et al.*[57], within the context of studying the kinetics of ordering in Ni_3Al alloyed with a third element (Nb, Ti, V, W, Cr, Co, Fe), measured the lattice parameters. Single phase Ni_3Al-based alloys were made using the Bridgman technique and annealed at 1500 K. The lattice parameters were then measured at 293 K. The authors present the chemical composition of the constituents of each crystal, however, no information about the site-occupation number is given. Since the Ni-composition of the alloys containing Nb, V, Ti and W is fixed to 75 at. % and the Al-composition of the alloy

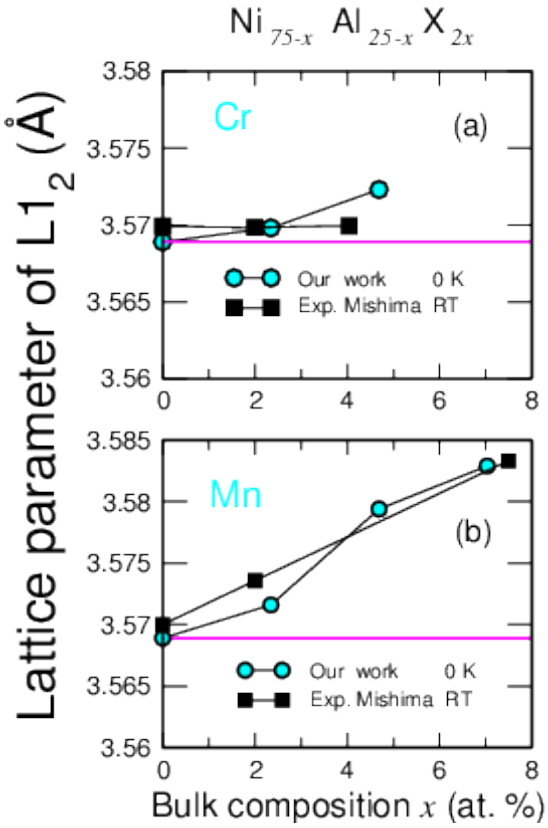

FIG. 3. The equilibrium lattice parameter of the alloy $Ni_{75-x}Al_{25-x}X_{2x}$ evolution as a function of the ternary element composition x (at. %). The RT experimental data from Ref. 35 are shown in each panel. The lines connecting the points are only to help guiding the eyes through the data.

containing Co is fixed to 25 at. %, we adopt the same assumption made by Morinaga *et al.*[56] to have an approximate idea about the site-preference behavior. Consequently, we present the lattice parameter of the alloys containing Nb, V, Ti and W on the Al-sites substitution graph and that of Co on the Ni-site.

2. *Experimental versus theoretical lattice parameters*

Figs. 1,2,3 show our 0 K predictions of the variation of the equilibrium lattice constants in the quasi-binary alloys: $Ni_{75-x}X_xAl_{25}$, $Ni_{75}Al_{25-x}X_x$ and $Ni_{75-x}Al_{25-x}X_{2x}$ alongside the available experimental data[35, 56, 57, 59]. Only Mishima *et al.*[35] provide data for several compositions per alloy giving us an idea how the lattice parameter qualitatively behaves as a function of alloying composition. On the other hand, Refs. 56 and 57 present the data of one single composition per alloy; these data can be used merely as an indicative of the magnitude of the change in lattice parameter due to a specific alloying composition.
Our zero K data qualitatively resemble the experimental[35] RT lattice parameter compositional

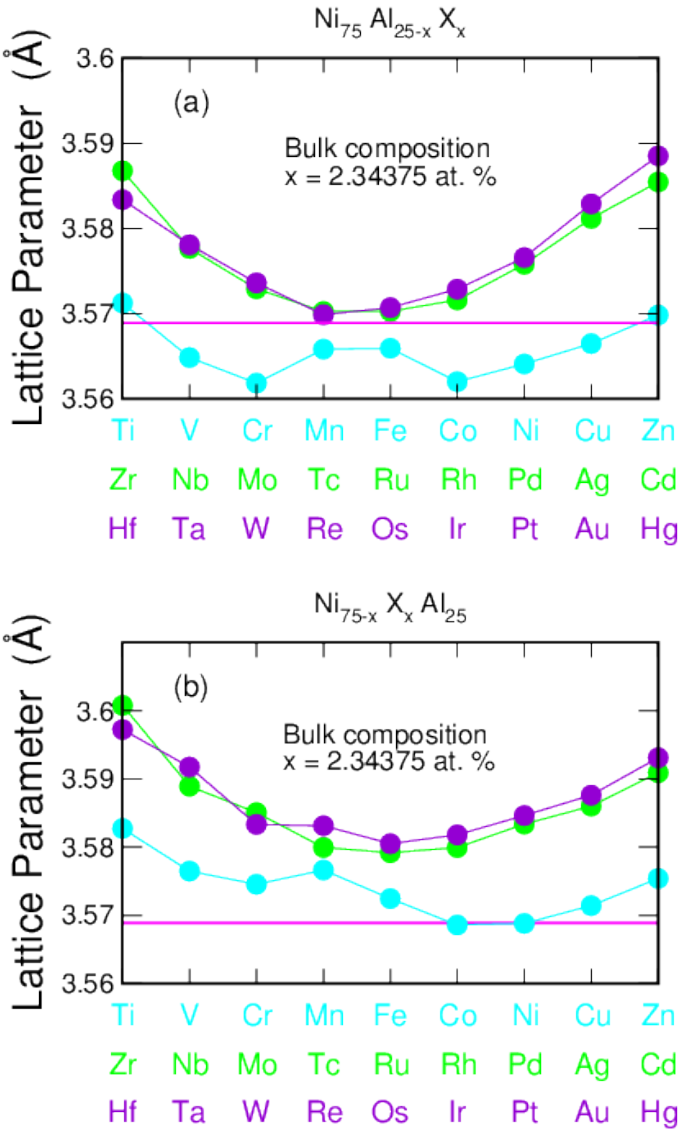

FIG. 4. The equilibrium lattice parameter of the alloy $Ni_{75}Al_{25-x}X_x$ and $Ni_{75-x}X_xAl_{25}$ as a function of the alloying element d-electron count at the composition 2.34375 at. %. The magenta line in each panel designates Ni_3Al. The lines connecting the points are only to help guiding the eyes through the data.

dependence. Apart from the alloy $Ni_{75-x}Al_{25-x}Fe_{2x}$, the maximum difference between our 0 K and the experimental data is ∼0.36 % occurring in the alloy $Ni_{75}Al_{25-x}Ti_x$ around the composition 12 at.%, which is understood as the experimental data are measured at RT where the thermal expansion is not negligible. In accordance with Mishima *et al.*[35], we predict the change in the lattice parameter in the alloys $Ni_{75-x}Co_xAl_{25}$ and $Ni_{75-x}Al_{25-x}Cr_{2x}$ to be very small. On the other hand, all the other alloys manifest a linear compositional dependence similarly to their variation at RT[35].
In general, one can understand the predicted and observed increase/decrease of the lattice parameter

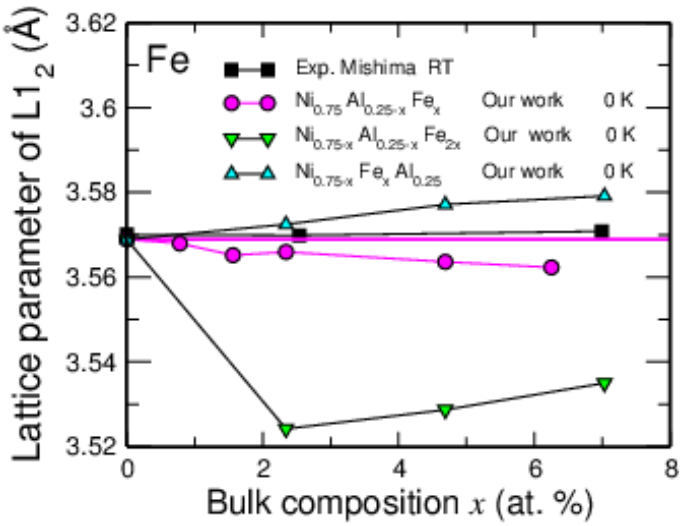

FIG. 5. The variation of the equilibrium lattice parameter as a function of alloying composition x for the $L1_2$ Ni-Al-Fe system. Our 0 K data correspond to alloys depending on the Fe site-preference. The lines connecting the points are only to help guiding the eyes through the data.

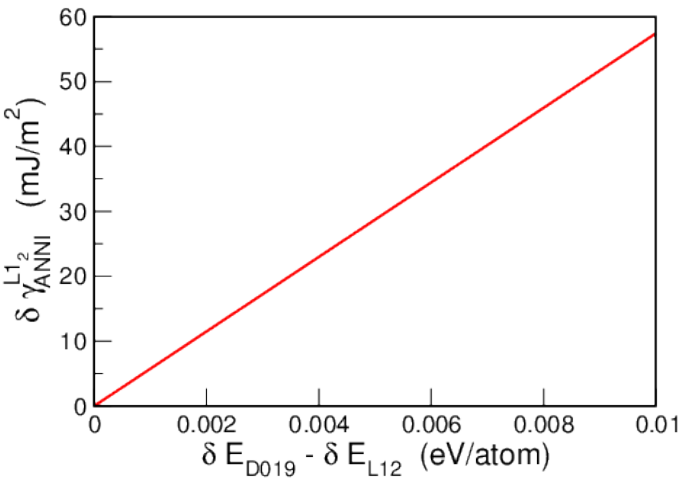

FIG. 6. The error in SISF energy, $\delta\gamma^{L1_2}_{ANNI}$, as a function of the error in determining the lowest energy configurations for $L1_2$ and $D0_{19}$ structures, $\delta E_{D0_{19}} - \delta E_{L1_2}$.

with composition in terms of the atomic size difference between the Ni/Al and the substituting ternary element. This is often called the geometric or atomic size argument[60]. For instance, larger Ti (Pd) atoms occupying smaller Al(Ni)-sites induce an increase in the alloy lattice parameter and smaller V atoms occupying larger Al-sites induce a reduction. In order to understand the differences in the composition variation of the alloy lattice parameter among the different systems, we try to identify a possible relation between the alloying element position in the periodic table and the alloy lattice parameter. To see the trend, we need to consider elements across the periodic table *i.e*, 3, 4 and 5d transition metal TM series - not only those shown in Figs. 1, 2 and 3. In Fig. 4 we establish the variation of the alloy lattice parameter as a function of the alloying element d-electron count for the alloy composition 2.34375 at. %. We observe a minimum lying toward the center of the TM series. This minimum is highly pronounced for 4 and 5d band series. The fluctuation exhibited across the 3d series is attributed to the strong magnetic nature of its elements, namely Cr/Mn/Fe/Co/Ni. This parabolic-minimum feature is related to the maximum cohesive-energy[61] of the elements located in the center relative to the periphery elements.

One can clearly recognize in Fig. 4 the dependence of the alloy lattice constant on the substitutional element atomic number for both Ni and Al-sites. This dependence shows that alloying Ni_3Al with TM elements residing toward the peripheries of the 4 and 5d periods yields an increase considerably larger than elements lying around the center. This explains how different ternary additions affect differently the lattice parameter as a function of alloying composition.

B. Superlattice intrinsic stacking fault energies

1. *SISF energy accuracy*

We have observed that $\gamma^{L1_2}_{ANNI}$ is extremely sensitive to energy difference between properly and unsatisfactorily relaxed $L1_2$ and $D0_{19}$ structures. As well stated in subsection III B we did not allow cell shape relaxations for both structures. Considering $L1_2$, at first we have relaxed the supercell volume keeping atomic positions fixed. Let's denote this as 1st step. In the 2nd step we set the volume of the supercell to the newly determined equilibrium volume and only allowed local atomic relaxations in order to find the configuration corresponding to minimum energy and forces. In the 3rd step, we updated the atomic positions to the new ones and relaxed again the supercell volume. We have repeated this procedure until the total energy changed no more. We found a significant energy difference between the 1st and the final step. This is due to the fact that the system has not yet converged into its lowest energetic configuration of volume and atomic-positions. Let's denote this energetic deviation between fully (final step) and non-converged (1st step) $L1_2$ structure (in terms of the true minimum) as δE_{L1_2}. Concerning $D0_{19}$, at first we performed a static calculation at its counterpart $L1_2$ volume-per-atom *i.e.*, atoms occupy their ideal $D0_{19}$ lattice sites and no volume relaxation (1st step). Next, we relaxed the $D0_{19}$ atomic positions also at its counterpart $L1_2$ volume-per-atom, in this way $D0_{19}$ is guaranteed to correspond to the underlying $L1_2$ lattice. The local atomic relaxations were repeated until no further energy change was noticed. Similarly to $L1_2$ we designate the energetic deviation between fully (final step) and non-converged (1st step) $D0_{19}$

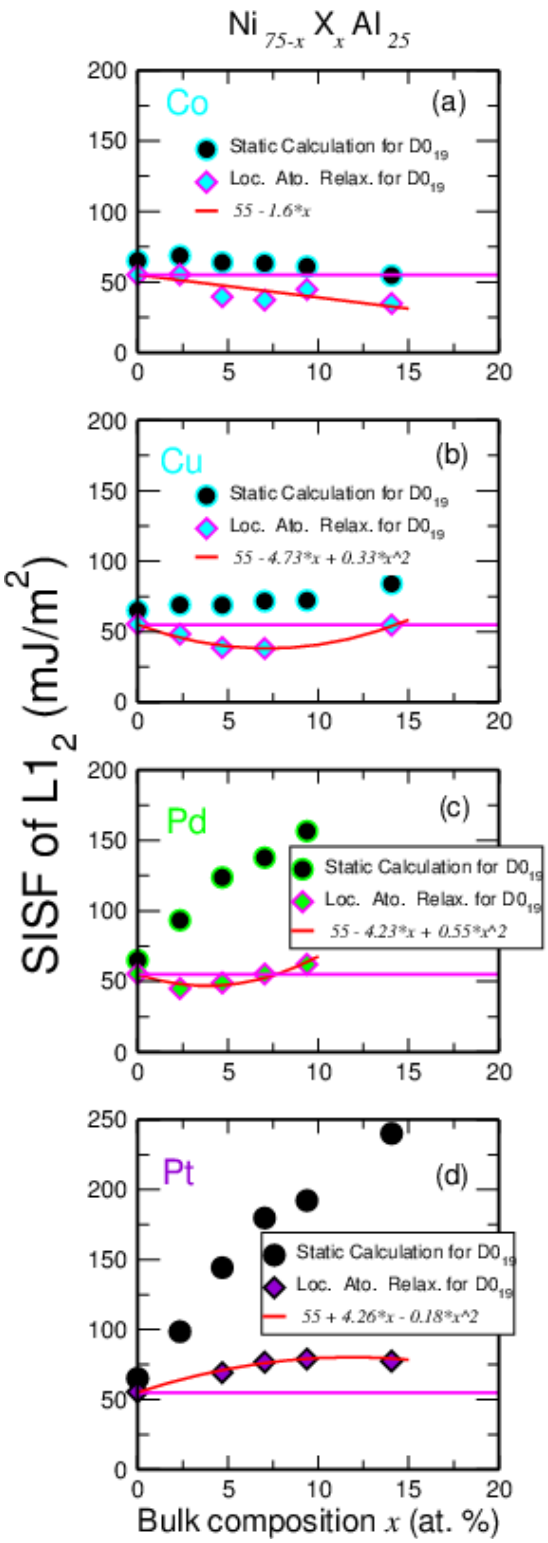

FIG. 7. Change in SISF energies due to introducing an alloying ternary element X with composition x uniquely to the Ni-sublattice. The solid red line symbolizes a fit to the pertinent data. The lines connecting the points are only to help guiding the eyes through the data.

structure in terms of the true minimum as $\delta E_{D0_{19}}$. Now Eq. 2 can be rearranged to include both energetic deviations δE_{L1_2} and $\delta E_{D0_{19}}$, and their impact on altering the magnitude of SISF energy,

$$\gamma^{L1_2}_{\rm ANNI} = \frac{8(E_{D0_{19}} - E_{L1_2})}{V^{2/3}_{L1_2}\cdot\sqrt{3}} + \frac{8(\delta E_{D0_{19}} - \delta E_{L1_2})}{V^{2/3}_{L1_2}\cdot\sqrt{3}} \quad . \tag{3}$$

the error is

$$\delta\gamma^{L1_2}_{\rm ANNI} = \frac{8(\delta E_{D0_{19}} - \delta E_{L1_2})}{V^{2/3}_{L1_2}\cdot\sqrt{3}} \quad . \tag{4}$$

We present in Fig. 6 the error in SISF energy, $\delta\gamma^{L1_2}_{ANNI}$, as a function of the absolute energetic deviation $\delta E_{D0_{19}} - \delta E_{L1_2}$. The fault-area term *i.e.* $A = V^{2/3}_{L1_2}\cdot\sqrt{3}$ depends on the alloying system, however, $\delta\gamma^{L1_2}_{ANNI}$ is not sensitive to the variation in the magnitude of fault-area. The minimum value of A is $21.6438\times10^{-20}m^2$ corresponding to $Ni_{0.75-x}Al_{0.25-x}Fe_{2x}$ (x=7.03125 at. %) and the maximum value is $23.0103\times10^{-20}m^2$ corresponding to $Ni_{0.75-x}Pt_xAl_{0.25}$ (x=14.0625 at. %), thus we set this term into an average value $22.32705\times10^{-20}m^2$.
As shown Fig. 6, an absolute energy difference as small as 0.01 eV/atom or 0.965 kJ/(mol·at.) can produce a 57 mJ/m^2 error in SISF energy - a large value. In point of fact, such an error is most likely to occur with the state-of-the-art available first-principles methods if one does not meticulously search for the lowest energy configurations of $L1_2$ and $D0_{19}$ considering all allowed types of relaxations.
The above discussion explains the large deviation between SISF energy data presented in Fig. 7, 8 and 9. The largest difference is observed for the alloy $Ni_{0.75-x}Pt_xAl_{0.25}$ where it reaches about 162 mJ/m^2 at 14.0625 at. %Pt. This arises from the energy difference between the static and atomic-positions-relaxed calculations of $D0_{19}$ structure; at that particular composition $\delta E_{D0_{19}}$ is 0.0291 eV/atom. This difference is understood because Pt atoms characterized by large Wigner-Seitz (WS) [62] radii (1.5319 Å) are substituting small Ni atoms (WS=1.3756 Å) and this atomic-size mismatch will induce an important atomic relaxations leading the system into its lowest energy configuration which is very much different from that of static calculations.

2. *Zero Kelvin SISF energy*

In Fig. 7, 8 and 9 we present the variation of SISF energies as a function of alloying composition x. We have computed the SISF energies for a range of alloying compositions limited to the maximum solubility of each ternary element X in γ'-Ni_3Al[35]. The figures are classified into three categories depending on the site preference of the alloying element X. For each alloy we present two

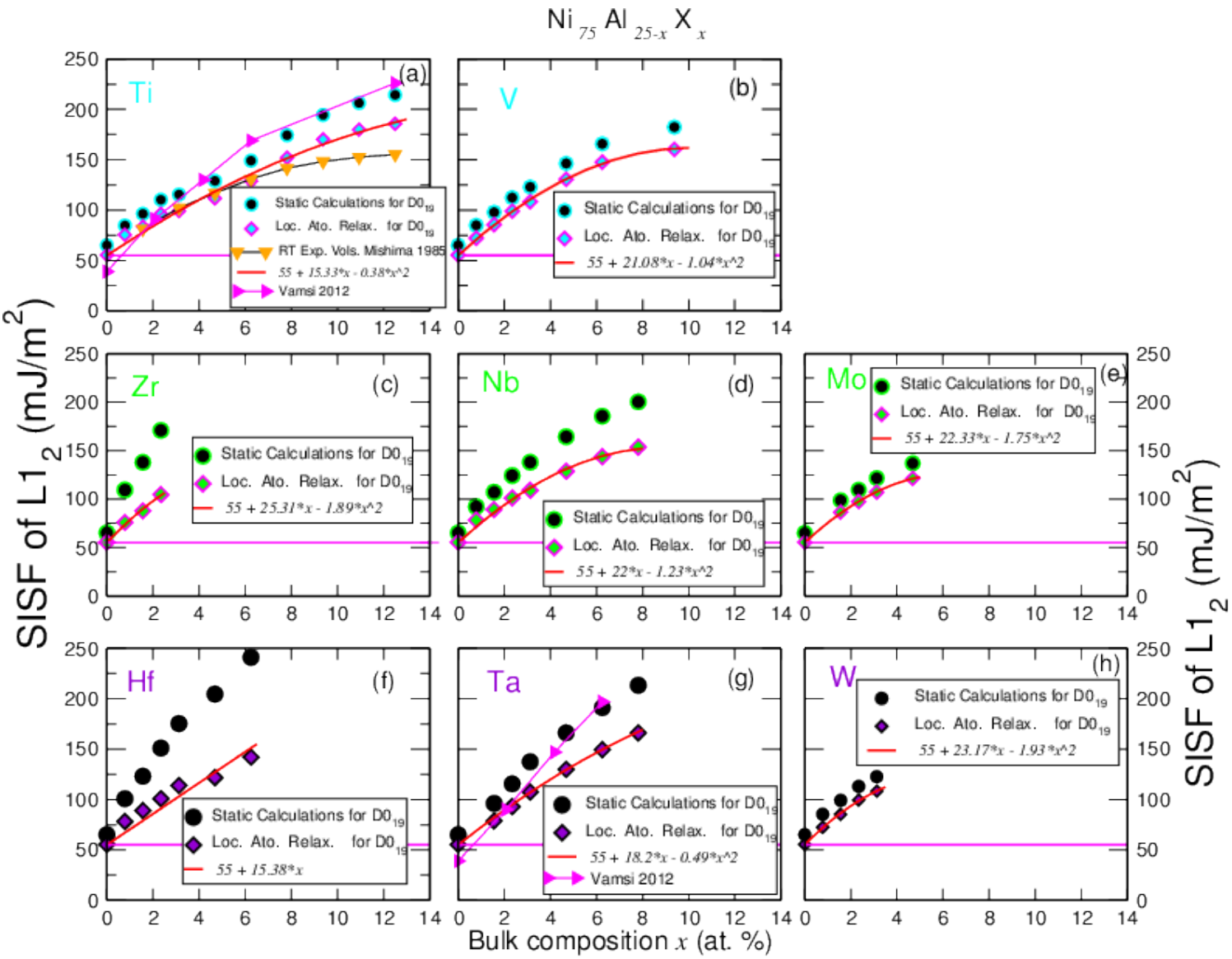

FIG. 8. Variation in SISF energies upon introducing an alloying ternary element X with composition x exceptionally to the Al-sites. The solid red line symbolizes a fit to the pertinent data. In panel (a), the down-ward orange triangles represent our calculations for the SISF energy at the RT experimental volumes[35]. The lines connecting the points are only to help guiding the eyes through the data.

data sets: one done with $D0_{19}$ phase atomic positions occupying their ideal lattice sites *i.e*, static calculation of the energy, while the second data set corresponds to energy of $D0_{19}$ phase where local atomic relaxations were performed in order to minimize forces on atoms within the the supercell. The purpose from presenting both data sets is to give a sense of magnitude of the large impact of relaxing $D0_{19}$ atomic positions on SISF energy for some ternary elements. Also, this kind of comparison is missing in literature work using AIM. The results that should be compared against experiment are those with atomic positions relaxed. From here onwards (until the end of this section) the discussion is related to SISF energy results corresponding to those obtained with relaxing the $D0_{19}$ structure.

As manifested in the figures, the extent of the sensitivity of SISF energies to chemical composition is considerable and for some alloys is remarkable. For instance $\sim$ 4 at .% Fe increases Ni_3Al SISF energy by 150 mJ/m^2. We should mention that our predicted SISF energies correspond to the situation where the ternary element composition is homogeneous throughout the fault region and the bulk. This is due to the fact that the applied AIM is a mean field approach based on comparing energies of two bulk structures. Therefore, one can not account for possible compositional variation (local concentration or enrichment of the ternary element) across the fault region with this model because the fault is not treated

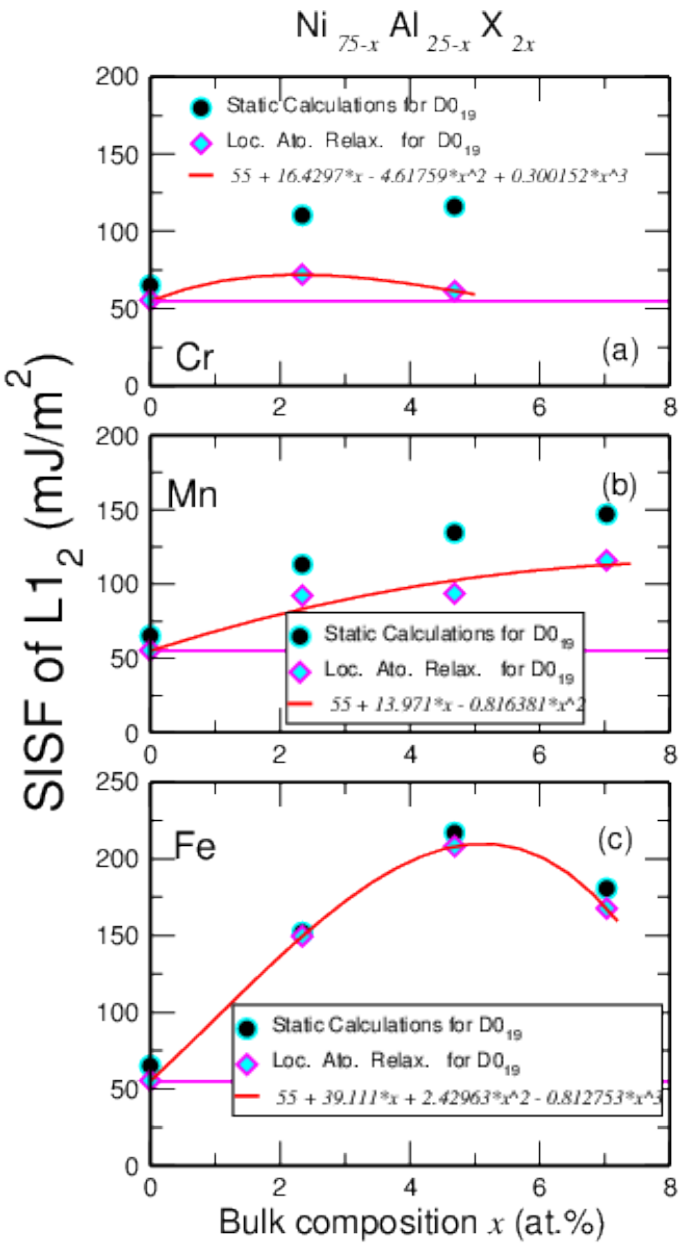

FIG. 9. Change in SISF energies for the case where same number of ternary added atoms go to both sublattices. The solid red line symbolizes a fit to the pertinent data. The lines connecting the points are only to help guiding the eyes through the data.

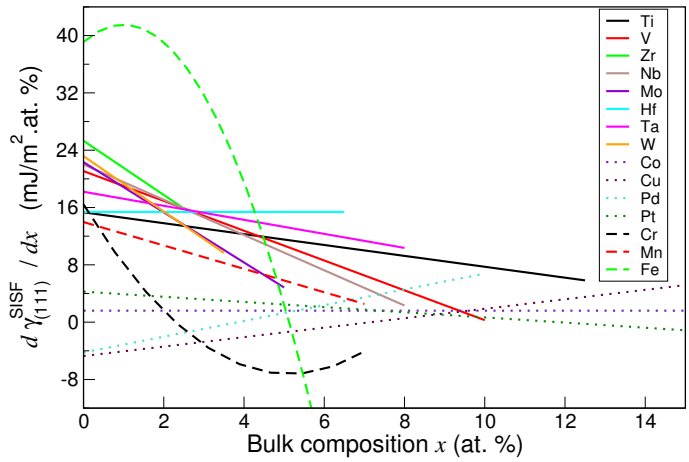

FIG. 10. SISF energy change rate with respect to alloying composition x.

explicitly. In fact, it has been shown recently[28] using energy dispersive X-ray spectroscopy (EDS), of two commercial superalloys (CMSX-4 and ME3), that some alloying elements notably Co and Cr segregate to the intrinsic stacking fault region within γ' precipitate, thus inducing a significant compositional variation in the vicinity of the fault. Later, Eurich and Bristowe[31] investigated using first-principles calculations the segregation behaviour of several alloying elements, confirming Co and Cr segregation to the fault. They found[31] that high alloy compositions of segregating elements can change the SISF energy in Ni_3Al by up to 126 mJ/m^2. Hence, one expects that the difference in SISF energy between direct supercell approach (accounting for local composition across the fault relative to the bulk) and the AIM model to be significant for alloys with high concentration of segregating elements, such as Co and Cr.

In Fig. 8 (a) and (g), we plot SISF energies change due to Ti and Ta additions, reported by Vamsi and Karthikeyan[32] using direct supercell approach. These SISF energies were determined through considering explicitly the stacking fault. For both Ti and Ta, our SISF energy composition dependence trend is consistent with their predictions. This could largely due to the fact that they employed a procedure to ensure the alloy composition across the fault and in the bulk are identical.

On the other hand, the striking increase of SISF energy upon alloying for most of the added elements X, except for Co, Cu and Pd is in contrast with the situation in γ-Ni where the stacking fault is characterized by an important reduction when introducing an alloying element X[63]. The increase in SISF energy in γ' comes as a penalty for lowering its high state of structural order. Adding chemical elements like Ti, Nb, Ta and V will increase the stability of the perfect $L1_2$ structure with respect to the distorted one. The hexagonal-close-packed like environment, within a $L1_2$ structure, is thus not favorable *via* alloying, except for cobalt. Most of the alloying elements induce a sublinear increase, whereas Cu and Pd produce a downward bowing with respect to the γ'-Ni_3Al SISF energy (55 mJ/m^2). On the other hand, Cobalt, causes a monotonic decrease in the SISF energies, reducing the SISF energy from 55 to 20 mJ/m^2 at its approximate maximum soluble composition (14.0625 at. %). This amounts to $\sim$ 37 % decrease. In fact, it is experimentally known that cobalt, particularly, promotes primary creep while tantalum suppresses it[1, 64]. Moreover, recently it has been shown that the decrease in stacking fault energy due to the increase of Co in Ni-

base superalloys (creep tested at 998 K/630 MPa) can promote dislocation dissociation and stacking fault formation in the matrix[65]. Our prediction of an increase in SISF energy upon introducing Ta into the Al-sublattice resonates with the experimental observation that Ta suppresses primary creep[66].

The significant increase in the SISF energy due to alloying, particularly, ternary elements known to preferentially partition to γ' such as Ti, Nb, Ta, and V explain why γ' precipitates can not be penetrated by dislocations [67] at low stresses. Our prediction of an increase in SISF energies with alloying explain the experimental fact that primary creep (occurring *via* stacking fault shearing of γ' precipitates) can only start at applied stresses higher than 500 MPa[5, 28]. Hence the primary effect, of an increase in SISF energy, due to alloying is only overcome at the combined conditions of intermediate temperature (1023 K[28]) and high stresses (750 MPa[28]). The applied stresses impose a considerable strain (8.6 %[28]) on the γ' lattice reducing thus the energy needed to form the fault, leading eventually to dislocations penetrating the γ' *via* stacking fault shearing mechanism. However, our results do not explain the secondary effect (following creep deformation) of alloying elements and their alloying compositions on creep properties, where it was recently[28] suggested that the formation of SISF fault regions is associated with long-range diffusion of Co/Cr segregants. The long range diffusion of these elements (Co/Cr) was suggested[28] to be intimately involved in the precipitate shearing process and is therefore closely linked to the time-dependent deformation of the alloys.

Let us mention here that Gorbatov *et al.*[68] , using the Coherent potential Approximation in conjunction with DFT, have predicted (010) and (111) APB energies in γ' to strictly increase as a function of alloying compositions of Ti, V, Cr and Cu. This increase in SISF and APB[68] formation energies elucidate the role played by γ' precipitates as effective barriers to the moving dislocations, leading to the unique high temperature creep properties in Ni-superalloys.

On the other hand, our (111) SISF are lower than (111) APBs[68] energies. This is due to the fact that in the case of creation of an SISF there is no change in the first and second nearest neighbours (1^{st}NN and 2^{nd}NN), change only happens in the third nearest neighbours 3^{rd}NN. Whereas creation of (111) APB causes a change in 1^{st}NN and 2^{nd}NN. Since 1^{st}NN and 2^{nd}NN interactions are stronger than 3^{rd}NN interactions, (111) APBs formation energies are greater than (111) SISF ones. This important difference is in line with experimental observation of the stability of SISF relative to APB energies[65, 69]. As a matter of fact, when dislocations shear γ' precipitates during plastic creep deformation, there will be different high energy configurations such as APB and complex stacking fault CSF. These high energy configurations would convert into SISF and SESF (superlattice extrinsic stacking fault) which possess lower energies in γ' precipitates during creep deformation[69].

We plot in Fig. 10 the SISF energy change rate, $d\gamma_{111}^{SISF}/dx$, with respect to alloying composition x. All alloying elements substituting for Al sites manifest a positive decreasing linear dependence, except Hf, it has a constant rate value. Elements substituting for Ni sites show negative and positive linear dependence depending on alloy composition. The strong compositional dependence of SISF energy rate reflects the nontrivial variation of SISF energies as a function of x. Hence, attempting to establish the SISF energy variation in Ni_3Al-based alloys using a naïve consideration of few highly-stoichiometric compositions, instead of finer compositional changes, and interpolating in-between in order to get access to the low composition region, is not possible.

3. *Temperature effect*

We have employed a quasistatic approach to calculate (111) SISF energy temperature dependence in $L1_2$ Ni_3Al-based alloys. This approach is based on the assumption that the change in SISF energy upon increasing temperature is solely due to thermal expansion and it has been successfully used to calculate the elastic constants of Ni_3Al[70, 71]. There are plentiful experimental evidences[72–74] supporting this approximation. This approach is also supported by a theoretical investigation[75] on Ta where the thermal expansivity was reported to be the main contribution of temperature to the elastic constants, while other thermal effects such as phonon and electronic excitation contributions were found to be quite small at constant volume. It has been as well successfully used to calculate SISF energies in unaries[22] and alloys[23] characterized by complex magnetic structures. The SISF energy temperature dependence was established using Eq. 2 by determining the energies of $L1_2$ and $D0_{19}$ phases at $L1_2$ equilibrium volume V corresponding to a temperature T. The volume temperature-dependence $V(T)$ was established using a quasiharmonic Debye model[76].

In order to have a preliminary idea of the temperature effect on the SISF energies we have done nonSP calculations for $Ni_{0.75-x}X_xAl_{0.25}$ alloys, due to the fact that it is computationally less demanding than SP scheme. However, only for the system $Ni_{0.75-x}Cu_xAl_{0.25}$, calculations were performed with both SP and nonSP schemes. The alloys were modeled using 108-atom $L1_2$-based 3×3×3(×4- atoms) and 216-atom $D0_{19}$-based 3×3×3(×8-atoms) supercells. The different size of these supercells from those used in the previous sections resulted in a set of different compositions. We should emphasize here that we have not relaxed the atomic positions of the $D0_{19}$ structure.

In order to understand SP and nonSP impact on the SISF energy temperature dependence, we analyze the results of the system $Ni_{0.75-x}Cu_xAl_{0.25}$. While nonSP data are lower than SP ones for the all compositions at high temperatures, the difference diminishes as Cu composition

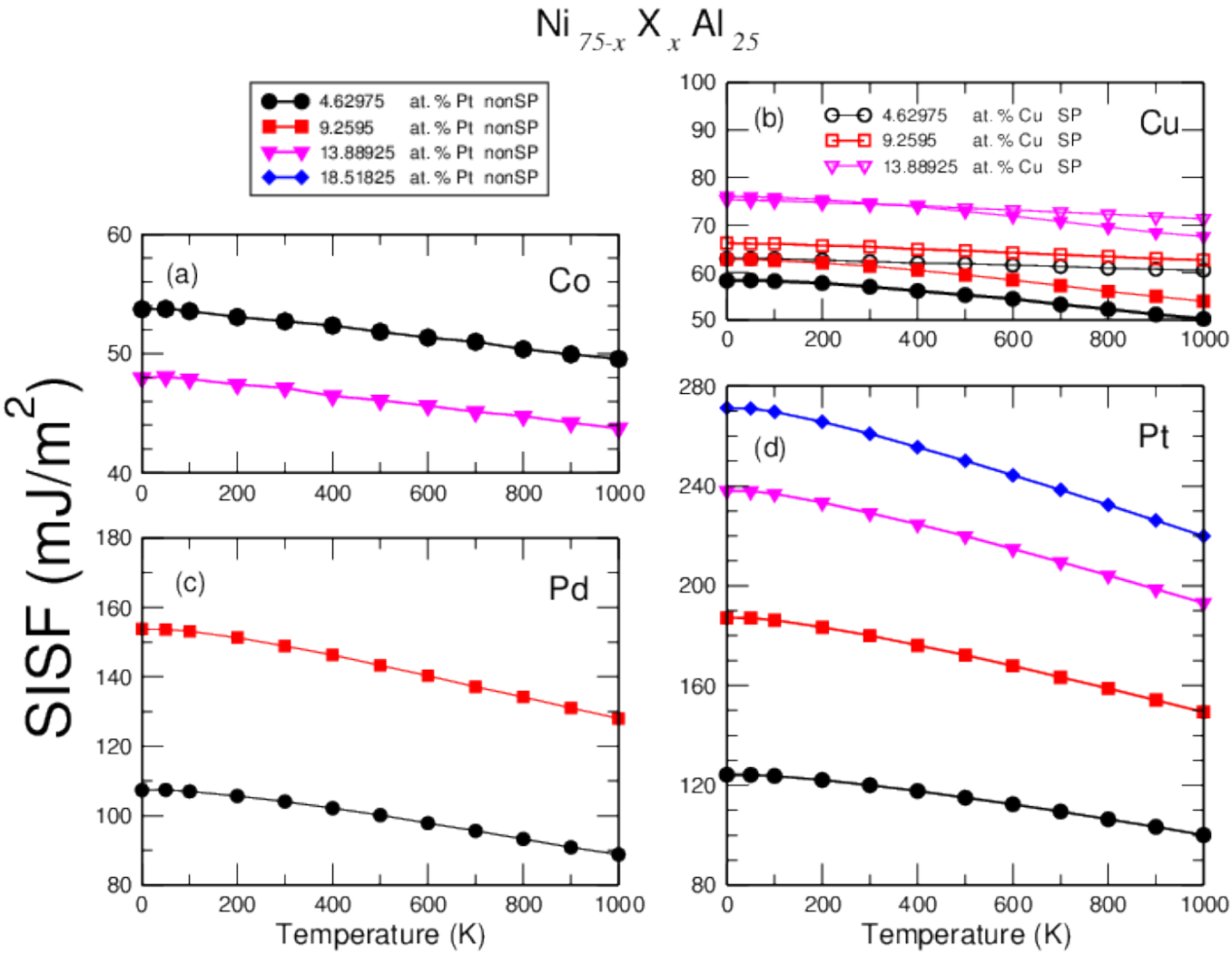

FIG. 11. Temperature dependence of SISF energies in $L1_2$ $Ni_{0.75-x}X_xAl$ alloys. The lines connecting the points are only to help guiding the eyes through the data.

increases. The maximum difference observed at 1000 K for the lowest composition 4.62975 at. % Cu is $\sim$ 17 %. This difference decreases to become $\sim$ 5 % for the highest composition 13.88925 at. % Cu, always at 1000 K. SISF energy variation with temperature features a quasilinear decrease in both schemes, nonSP data exhibit a sharper decrease at higher temperature, though.

One can notice that the decrease of SISF energy as a function of temperature is observed in the whole studied systems. Interestingly, we have recently[33] predicted similar decrease behavior of the SISF energies in the $L1_2$ compounds Ni_3(Al,Mn,Pt). While the decrease is relatively modest in $Ni_{0.75-x}Co_xAl_{0.25}$ and $Ni_{0.75-x}Cu_xAl_{0.25}$, it is quite significant in $Ni_{0.75-x}Pd_xAl_{0.25}$ and $Ni_{0.75-x}Pt_xAl_{0.25}$. For instance, the SISF energy is 271 mJ/m^2 at 0 K and 220 mJ/m^2 at 1000 K for the composition 18.51825 at. %Pt, this gives rise to a reduction as big as $\sim$ 19 %. However, this temperature-induced reduction in SISF energy, observed in the all alloys studied here, is not strong enough to decrease the SISF energies to negative or values close to zero. In fact, as we have demonstrated above that at the highest temperature studied here *i.e.*, 1000 K, SISF energy values of the different systems stay relatively close to their 0 K values. This helps explaining the remarkable stability of Ni_3Al-based alloys at high temperatures.

On the other hand, relaxing the atomic positions of $D0_{19}$ structure will reduce the SISF energy values, similarly to what we observe in Fig. 7, particularly for systems with Pd and Pt as ternary additions. But we don not think it will have a *qualitative* effect on the temperature dependence of the SISF energies *i.e.*, we do not expect to have

an increase instead of the observed decrease or to have negative or values closer to zero. We plan to establish this in a separate study in the future soon.

We have as well calculated, using the SP scheme, the SISF energies at the experimental room temperature RT lattice parameters[35] of $Ni_{0.75}Al_{0.25-x}Ti_x$ alloy, allowing atomic positions of both $L1_2$ and $D0_{19}$ structures to relax. As shown in Fig. 8(a) the SISF energies exhibit a significant decrease with respect to 0 K results for Ti-rich compositions ($x \geqslant 9.375$ at. %). It is about 30 mJ/m^2 at the maximum calculated composition (12.5 at. %). For Ti compositions lower than 7.8125 at. %, the difference between 0 K and RT SISF energies is almost negligible (≤ 3 mJ/m^2).

In summary, the change in SISF energies overall due to alloying is more pronounced than temperature effect. In fact, most X elements in this study, except those substituting for Ni-sites, induce over 100 % increase in SISF energies starting from a composition as small as 2 at. %. However, taking into account the considerable decrease in SISF energy in some of the studied alloys, it seems that the combined effect of alloying and temperature is very interesting to heavily explore in an independent study.

V. CONCLUSIONS

Ab initio calculations have been done to establish the lattice parameter and the SISF energy variation as a function of finer compositional changes x for Ni_3Al-based alloys. Apart from Fe and Co, all the ternary additions result in a linear increase in the lattice parameter as a function of composition x; except vanadium, its compositional dependence reduces monotonically the lattice parameter.

On the other hand, iron and all ternary elements substituting for Al site induce an important increase in the SISF energy, which is in contrast with the scenario in γ-Ni where the stacking fault energy is reduced upon introducing an alloying element. This increase enhances γ' precipitates resistance against shearing and consequently improves Ni-superalloys high-temperature strength. Only Co decreases monotonically the SISF energy, facilitating the stacking fault shear of γ' precipitates and thus promoting primary creep. We have established the analytical dependence of the SISF energies on the ternary element composition x limited to its solubility limit. Our ternary functional composition dependence of (111) SISF energies for pseudo-binary systems are extremely important to improve state of the art physics-based deformation models of primary creep, since the compositional dependence of SISF energies in pseudo-binary systems offer the possibility to fine-tune the SISF energies of a multicomponent alloy and thereby optimizing its creep resistance. Our preliminary calculations for thermal effect show that SISF energies decrease with temperature and this decrease becomes more important at increasing alloying compositions. While the present results represent a significant advance in stacking fault calculations in alloys, further improvements must include temperature and short range order effects.

ACKNOWLEDGMENTS

We would like to thank Professor Andrei Ruban (KTH university) and Professor Andrei Postnikov (Université de Lorraine) for carefully reading the manuscript and for useful suggestions. This work used the ARCHER UK National Supercomputing Service (http://www.archer.ac.uk), University of Birmingham's BlueBEAR HPC service (http://www.birmingham.ac.uk/bear), and computing resources through the MidPlus Regional HPC Center, we therefore would like to acknowledge them. Also, we would like to acknowledge the EPSRC (grant EP/M021874/1) and EU FP7 (grant GA109937) for financial support.

[1] R.C. Reed, *Superalloys: Fundamentals and Applications* (Cambridge University Press, Cambridge, 2006).

[2] T.M. Pollock and S.J. Tin, Propul. Power **22**, 361 (2006).

[3] N. Matan, D.C. Cox, P. Carter, M.A. Rist, C.M.F. Rae, and R.C. Reed, Acta Materialia **47**, 1549 – 1563 (1999), http://www.sciencedirect.com/science/article/pii/S1359645499000294.

[4] B. H. Kear, J. M. Oblak, and A. F. Giamei, Metallurgical Transactions **1**, 2477–2486 (1970), http://dx.doi.org/10.1007/BF03038373.

[5] C.M.F. Rae and R.C. Reed, Acta Materialia **55**, 1067 – 1081 (2007), //www.sciencedirect.com/science/article/pii/S1359645406006847.

[6] G. R. Leverant and B. H. Kear, Metallurgical Transactions **1**, 491–498 (1973).

[7] C.M.F. Rae, N. Matan, and R.C. Reed, Materials Science and Engineering: A **300**, 125 – 134 (2001), ISSN 0921-5093, http://www.sciencedirect.com/science/article/pii/S0921509300017883.

[8] L. Kovarik, R.R. Unocic, Ju Li, P. Sarosi, C. Shen, Y. Wang, and M.J. Mills, Progress in Materials Science **54**, 839 – 873 (2009), http://www.sciencedirect.com/science/article/pii/S0079642509000139.

[9] G.B. Viswanathan, P.M. Sarosi, M.F. Henry, D.D. Whitis, W.W. Milligan, and M.J. Mills, Acta Materialia **53**, 3041 – 3057 (2005), ISSN 1359-6454, http://www.sciencedirect.com/science/article/pii/S1359645405001655.

[10] G. Vanderschaeve, Philosophical Magazine A **56**, 689–701 (1987), http://dx.doi.org/10.1080/01418618708204482.

[11] G. Schoeck, S. Kohlhammer, and M. Fahnle, Philosophical Magazine Letters **79**, 849–857 (1999).

[12] A. Suzuki and T. M. Pollock, Acta Materialia **56**, 1288–1297 (2008).

[13] M. Chandran and S. K. Sondhi, Journal of Applied Physics **109**, 1–6 (2011).

[14] S. Ogata, J. Li, and S. Yip, Science **298**, 807–811 (2002).

[15] J. R. Rice and G. E. Beltz, J. Mech. Phys. Solids **42**, 333 (1994).

[16] P. J. H. Denteneer and W. van Haeringen, Journal of Physics C: Solid State Physics **20**, L883 (1987), http://stacks.iop.org/0022-3719/20/i=32/a=001.

[17] S. Lu, Q-M Hu, B. Johansson, and L. Vitos, Acta Materialia **59**, 5728 – 5734 (2011), //www.sciencedirect.com/science/article/pii/S1359645411003892.

[18] L. Vitos, P. A. Korzhavyi, J-O Nilsson, and B. Johansson, Physica Scripta **77**, 065703 (2008), http://stacks.iop.org/1402-4896/77/i=6/a=065703.

[19] L. Vitos, P. A. Korzhavyi, and B. Johansson, Phys. Rev. Lett. **96**, 117210 (Mar 2006), http://link.aps.org/doi/10.1103/PhysRevLett.96.117210.

[20] L. Vitos, J.-O. Nilsson, and B. Johansson, Acta Materialia **54**, 3821–3826 (2006), //www.sciencedirect.com/science/article/pii/S1359645406002989.

[21] T. Gebhardt, D. Music, M. Ekholm, I. A. Abrikosov, L. Vitos, A. Dick, T. Hickel, J. Neugebauer, and J. M. Schneider, Journal of Physics: Condensed Matter **23**, 246003 (2011), http://stacks.iop.org/0953-8984/23/i=24/a=246003.

[22] I. Bleskov, T. Hickel, J. Neugebauer, and A. Ruban, Phys. Rev. B **93**, 214115 (2016), http://link.aps.org/doi/10.1103/PhysRevB.93.214115.

[23] V. I. Razumovskiy, A. Reyes-Huamantinco, P. Puschnig, and A. V. Ruban, Phys. Rev. B **93**, 054111 (Feb 2016), http://link.aps.org/doi/10.1103/PhysRevB.93.054111.

[24] A. Reyes-Huamantinco, P. Puschnig, C. Ambrosch-Draxl, O. E. Peil, and A. V. Ruban, Phys. Rev. B **86**, 060201 (Aug 2012), http://link.aps.org/doi/10.1103/PhysRevB.86.060201.

[25] M. Rahaman, V. I. Razumovskiy, B. Johansson, and A. V. Ruban, Philosophical Magazine **93**, 3423–3441 (2013), http://dx.doi.org/10.1080/14786435.2013.810817.

[26] H. Suzuki, Journal of the Physical Society of Japan **17**, 322–325 (1962), http://dx.doi.org/10.1143/JPSJ.17.322.

[27] T. Hickel, S. Sandlöbes, R.K.W. Marceau, A. Dick, I. Bleskov, J. Neugebauer, and D. Raabe, Acta Materialia **75**, 147 – 155 (2014), //www.sciencedirect.com/science/article/pii/S1359645414003255.

[28] G.B. Viswanathan, R. Shi, A. Genc, V.A. Vorontsov, L. Kovarik, C.M.F. Rae, and M.J. Mills, Scripta Materialia **94**, 5 – 8 (2015), ISSN 1359-6462, http://www.sciencedirect.com/science/article/pii/S1359646214002632.

[29] Xiao-Xiang Yu and Chong-Yu Wang, Materials Science and Engineering: A **539**, 38 – 41 (2012), //www.sciencedirect.com/science/article/pii/S0921509312000391.

[30] S. L. Shang, W. Y. Wang, Y. Wang, Y. Du, J. X. Zhang, A. D. Patel, and Z. K. Liu, Journal of Physics: Condensed Matter **24**, 155402 (2012), http://stacks.iop.org/0953-8984/24/i=15/a=155402.

[31] N.C. Eurich and P.D. Bristowe, Scripta Materialia **102**, 87 – 90 (2015), ISSN 1359-6462, http://www.sciencedirect.com/science/article/pii/S1359646215000743.

[32] K. V. Vamsi and S. Karthikeyan, in *Superalloys 2012* (John Wiley & Sons, Inc., 2012) pp. 521–530, http://dx.doi.org/10.1002/9781118516430.ch57.

[33] A. Breidi, J. Allen, and A. Mottura, physica status solidi (b) **254**, n/a–n/a (2017), ISSN 1521-3951, http://dx.doi.org/10.1002/pssb.201600839.

[34] L. Vitos, P. A. Korzhavyi, and B. Johansson, Phys. Rev. Lett. **96**, 117210 (Mar 2006), http://link.aps.org/doi/10.1103/PhysRevLett.96.117210.

[35] Y. Mishima, S. Ochiai, and T. Suzuki, Acta Metallurgica **33**, 1161 – 1169 (1985), http://www.sciencedirect.com/science/article/pii/0001616085902111.

[36] In $Ni_{0.75-x}X_xAl_{0.25}$ system, x=2.34375 at.% was modeled using 256-atom $L1_2$-based 4×4×4(×4-atoms) and $D0_{19}$-based 4×4×2(×8-atoms) supercells.

[37] J. M. Cowley, Journal of Applied Physics **21**, 24–30 (1950), http://scitation.aip.org/content/aip/journal/jap/21/1/10.1063/1.1699415.

[38] B.E. Warren, *X-ray diffraction* (New York, Dover, 1990).

[39] Yiyou Tu, Zugang Mao, and David N. Seidman, Applied Physics Letters **101** (2012), doi: \bibinfo{doi}{http://dx.doi.org/10.1063/1.4753929}, http://scitation.aip.org/content/aip/journal/apl/101/12/10.1063/1.4753929.

[40] A. Almazouzi, H. Numakura, M. Koiwa, K. Hono, and T. Sakurai, Intermetallics **5**, 37 – 43 (1997), http://www.sciencedirect.com/science/article/pii/S0966979596000647.

[41] Andrei V. Ruban, V.A. Popov, V.K. Portnoi, and V.I. Bogdanov, Philosophical Magazine **94**, 20–34 (2014), http://dx.doi.org/10.1080/14786435.2013.838647.

[42] C. Jiang and B. Gleeson, Scripta Materialia **55**, 433 – 436 (2006), ISSN 1359-6462, http://www.sciencedirect.com/science/article/pii/S1359646206003903.

[43] A. V. Ruban and H. L. Skriver, Phys. Rev. B **55**, 856–874 (1997), http://link.aps.org/doi/10.1103/PhysRevB.55.856.

[44] P. Hohenberg and W. Kohn, Phys. Rev. **136**, B864–B871 (Nov 1964).

[45] W. Kohn and L. J. Sham, Phys. Rev. **140**, A1133–A1138 (Nov 1965).

[46] G. Kresse and D. Joubert, Phys. Rev. B **59**, 1758–1775 (Jan 1999), http://link.aps.org/doi/10.1103/PhysRevB.59.1758.

[47] G. Kresse and J. Furthmüller, Computational Materials Science **6**, 15 – 50 (1996), ISSN 0927-0256, http://www.sciencedirect.com/science/article/pii/0927025696000080.

[48] P. E. Blöchl, Phys. Rev. B **50**, 17953–17979 (Dec 1994), http://link.aps.org/doi/10.1103/PhysRevB.50.17953.

[49] J. P. Perdew, K. Burke, and M. Ernzerhof, Phys. Rev. Lett. **77**, 3865–3868 (Oct 1996).

[50] W.H. Press, S.A. Teukolsky, W.T. Vetterling, and B.P. Flannery (Cambridge University Press, 2007) ISBN 9780521880688, http://books.google.fr/books?id=1aA0dzK3FegC.

[51] A. Aguayo, I. I. Mazin, and D. J. Singh, Phys. Rev. Lett. **92**, 147201 (Apr 2004), http://link.aps.org/doi/10.1103/PhysRevLett.92.147201.

[52] S. T. Sekula, H. R. Kerchner, J. R. Thompson, and Th. Leventouri, MRS Proceedings **39** (1984).

[53] A. V. Ruban, S. Khmelevskyi, P. Mohn, and B. Johansson, Phys. Rev. B **75**, 054402 (Feb 2007), http://link.aps.org/doi/10.1103/PhysRevB.75.054402.

[54] T.M. Pollock and A.S. Argon, Acta Metallurgica et Materialia **42**, 1859 – 1874 (1994), ISSN 0956-7151, http://www.sciencedirect.com/science/article/pii/0956715194900116.

[55] A. Heckl, S. Neumeier, M. Göken, and R. F. Singer, Materials Science and Engineering: A **528**, 3435 – 3444 (2011), ISSN 0921-5093, http://www.sciencedirect.com/science/article/pii/S0921509311000311.

[56] M. Morinaga, K. Sone, T. Kamimura, K. Ohtaka, and N. Yukawa, Journal of Applied Crystallography **21**, 41–47 (1988), http://dx.doi.org/10.1107/S0021889887008975.

[57] O.V Savin, N.N Stepanova, Yu.N Akshentsev, and D.P Rodionov, Scripta Materialia **45**, 883 – 888 (2001), http://www.sciencedirect.com/science/article/pii/S1359646201010569.

[58] A. V. Ruban and V. I. Razumovskiy, Phys. Rev. B **86**, 174111 (Nov 2012), http://link.aps.org/doi/10.1103/PhysRevB.86.174111.

[59] P. V. Mohan Rao, K. Satyanarayana Murthy, S. V. Suryanarayana, and S. V. Nagender Naidu, physica status solidi (a) **133**, 231–235 (1992), ISSN 1521-396X, http://dx.doi.org/10.1002/pssa.2211330203.

[60] J.-C. Crivello, A. Breidi, and J.-M. Joubert, Inorganic Chemistry **52**, 3674–3686 (2013), http://dx.doi.org/10.1021/ic302142w.

[61] J. H. Rose and H. B. Shore, Phys. Rev. B **49**, 11588–11601 (May 1994).

[62] Equilibrium Wigner-Seitz radii (WS) can be derived from the room temperature (R.T.) experimental atomic volumes[77] ($V_{exp}^{RT} = \frac{4}{3}\pi WS^3$) of the alloying element ground state structure.

[63] S. L. Shang, C. L. Zacherl, H. Z. Fang, Y. Wang, Y. Du, and Z. K. Liu, Journal of Physics: Condensed Matter **24**, 505403 (2012), http://stacks.iop.org/0953-8984/24/i=50/a=505403.

[64] H. Murakami, T. Yamagata, H. Harada, and M. Yamazaki, Materials Science and Engineering: A **223**, 54 – 58 (1997), ISSN 0921-5093, http://www.sciencedirect.com/science/article/pii/S0921509396104949.

[65] Chenggang Tian, Guoming Han, Chuanyong Cui, and Xiaofeng Sun, Materials & Design **64**, 316 – 323 (2014), ISSN 0261-3069, http://www.sciencedirect.com/science/article/pii/S0261306914006128.

[66] G.L. Drew, R.C. Reed, K. Kakehi, and C.M.F. Rae, in *Superalloys 2004*, The Minerals, Metals & Materials Society), edited by K.A. Green, T.M. Pollock, H. Harada, T.E. Howson, R.C. Reed, J.J. Schirra, and S. Walston (2004) p. 127.

[67] Dislocations enter γ' through creating planar faults *via* stacking fault shearing mechanism as described in Ref. 5.

[68] O. I. Gorbatov, I. L. Lomaev, Yu. N. Gornostyrev, A. V. Ruban, D. Furrer, V. Venkatesh, D. L. Novikov, and S. F. Burlatsky, Phys. Rev. B **93**, 224106 (Jun 2016), http://link.aps.org/doi/10.1103/PhysRevB.93.224106.

[69] R. R. Unocic, *On the creep deformation mechanisms of an advanced disk nickel-base superalloy*, Ph.D. thesis, The Ohio State University (2008).

[70] Y Wang, J J Wang, H Zhang, V R Manga, S L Shang, L-Q Chen, and Z-K Liu, Journal of Physics: Condensed Matter **22**, 225404 (2010), http://stacks.iop.org/0953-8984/22/i=22/a=225404.

[71] Shun-Li Shang, Hui Zhang, Yi Wang, and Zi-Kui Liu, Journal of Physics: Condensed Matter **22**, 375403 (2010), http://stacks.iop.org/0953-8984/22/i=37/a=375403.

[72] C.A. Swenson, Journal of Physics and Chemistry of Solids **29**, 1337 – 1348 (1968), ISSN 0022-3697, http://www.sciencedirect.com/science/article/pii/0022369768901856.

[73] E.F. Wasserman, "Chapter 3 Invar: Moment-volume instabilities in transition metals and alloys," in *Handbook of Ferromagnetic Materials*, Handbook of Ferromagnetic Materials, Vol. 5 (Elsevier, 1990) pp. 237 – 322, http://www.sciencedirect.com/science/article/pii/S157493040580063X.

[74] Orson L. Anderson and Donald G. Isaak, "Elastic constants of mantle minerals at high temperature," in *Mineral Physics & Crystallography: A Handbook of Physical Constants* (American Geophysical Union, 2013) pp. 64–97, ISBN 9781118668191, http://dx.doi.org/10.1029/RF002p0064.

[75] O. Gülseren and R. E. Cohen, Phys. Rev. B **65**, 064103 (Jan 2002), https://link.aps.org/doi/10.1103/PhysRevB.65.064103.

[76] M.A. Blanco, E. Francisco, and V. Luaña, Computer Physics Communications **158**, 57 – 72 (2004), http://www.sciencedirect.com/science/article/pii/S0010465503005472.

[77] C. Kittel, *Introduction to Solid State Physics*, 7th ed. (Wiley, New York, 1996, 1996).